

Modelling and Simulation of Skid-equipped Shipboard Rotorcraft

Dr. Rob Langlois
Carleton University
Dept. Mech. & Aero. Eng.
1125 Colonel By Dr.
Ottawa, ON
Canada K1S 5B6
rlangloi@mae.carleton.ca

Dr. Zheng H. Zhu
York University
Dept. Earth & Space Sci. & Eng.
4700 Keele Street
Toronto, ON
Canada M3J 1P3
gzhu@yorku.ca

Michael LaRosa
Curtiss-Wright Controls Engineered
Systems - Marine Defense
3570 Hawkestone Road
Mississauga, ON
Canada L5C 2V8
michael.larosa@indaltech.com

Keywords: Dynamic interface analysis, shipboard aircraft operation, skid landing gear, Dynaface

Abstract

Mathematical modelling and computer simulation has proven to be the tool of choice for supporting the development and operation of shipboard aircraft securing and handling equipment. While other alternatives have been used for specific phases and aspects of operation, the variety of nonlinear effects present and range of analysis types that are required strongly support transient time-domain simulation as the most versatile option. The DYNAFACE[®] simulation program has been developed over the past fifteen years and is widely used for this purpose, particularly for the analysis of conventional shipboard aircraft designed with wheeled landing gears. Increasingly, a requirement has emerged for the ability to model shipboard aircraft having skid landing gear – both due to occasional use of land-based aircraft aboard ships and for supporting the design and operation of ship-based UAVs that are often fitted with skid landing gear. This paper describes in detail for the first time recent mathematical modelling resulting in the extension of DYNAFACE[®] capabilities to include the modelling of skid-equipped rotorcraft both using a fast linear stiffness modelling approach for the gear and using a more-general nonlinear finite element structural modelling approach. In both cases, an efficient skid/deck interface model is used. The two modelling options provide versatility in the type of analysis that can be performed. Sample results from a typical analysis are also presented and discussed.

1. INTRODUCTION

Dynamic interface analysis refers to the study of the effects of ship motion on all aspects of shipboard aircraft operation. This work is facilitated by transient dynamic computer simulation. Over the past fifteen years, Curtiss-Wright Controls Engineered Systems - Marine Defense developed the DYNAFACE[®] dynamic interface analysis simulation program that computes the time-domain response of shipboard aircraft to ship motion and wind while secured by aircraft handling equipment [1,2]. DYNAFACE[®], in its original form, was developed to model conventional maritime aircraft equipped

with wheeled landing gears. Increasingly, there is a need to analyze shipboard operation of aircraft fitted with skid landing gear. As a result, this research was undertaken to support this requirement.

The typical structural elements of a skid landing gear and associated nomenclature are defined in Figure 1. It is observed that the two main structural elements are the skid tubes and the cross-tubes. The cross-tubes provide the compliance in the landing gear and typically provide little damping to the system unless fitted with external damping devices. The skid-tubes serve the primary function of providing a large contact area with the ground and consequently minimize contact pressure. Some research has suggested that the compliance of the skid tubes may be small compared with that of the cross-tubes. Others [3,4,5] have studied the dynamic behaviour of landing gear and skid tubes using commercial nonlinear finite element packages. However, their models considerably simplified the aircraft dynamic model and ignored aerodynamic loads as the focus was on the landing gear design and performance. The extension made to DYNAFACE[®], and presented in this paper, includes two landing gear stiffness models. The first is a linear model that makes assumptions about the linearity of the landing gear stiffness and the relative rigidity of the skid-tubes. As a result, the associated input data requirement is simple and the simulation run speed is fast. The second alternative models the cross-tubes and skid-tubes using a general three-dimensional finite element analysis supporting beam elements. While more complex than the linear model, the input file remains fairly simple and this model provides considerable versatility in the range of landing gear that can be represented. The simulation speed, though much slower than the linear model, is not prohibitive in this transient-dynamic simulation due to the use of the finite element model strictly as a stiffness force producing device without implicitly including the high frequency vibration modes associated with full flexible body dynamic analysis and the corresponding numerical stiffness. In subsequent sections, an overview of the DYNAFACE[®] dynamic interface simulation program will be given, the theoretical underpinnings of each skid modelling approach will be described and comments about their implementation given, and sample analysis results will be

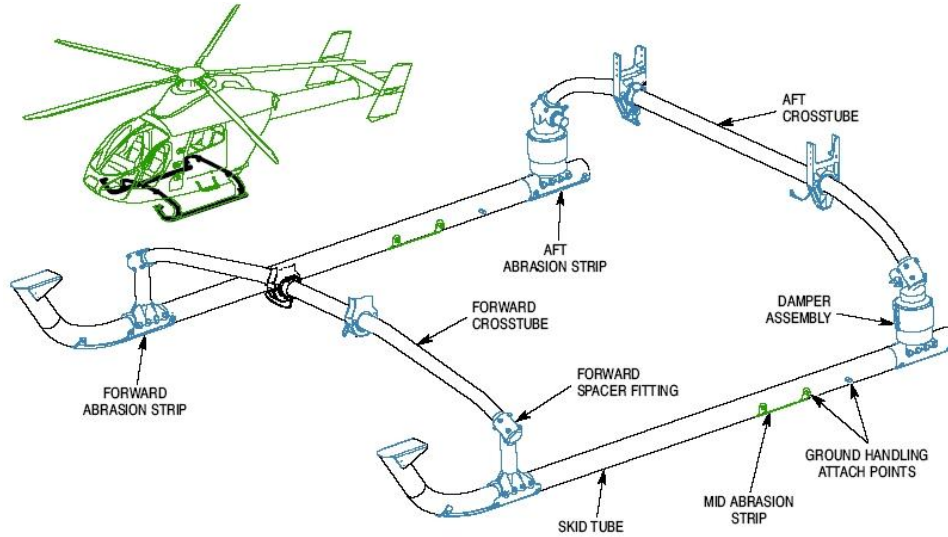


Figure 1. Skid aircraft landing gear nomenclature (adapted from [6])

presented and discussed.

2. DYNAFACE SIMULATION

DYNAFACE[®] consists of a special-purpose 16-degree-of-freedom mathematical model of the aircraft/ship system[1,2]. While the simulation is special purpose to promote solution efficiency, it includes sufficient generality such that a large variety of aircraft and virtually all ships can readily be modelled. In its original form, the simulation contains prismatic oleo and leading/trailing arm suspension models having up to two wheels each that can be attached to the fuselage in either nose wheel or tail wheel configurations, up to two main rotors, and a large variety of possible securing devices. The model includes detailed representations of the oleo stiffness, damping, and friction characteristics; wind-induced rotor forces and moments; and a detailed nonlinear tire model that supports complex tire behaviour including lift-off and touch-down, rolling due to suspension travel, brake slippage, and sliding.

Computationally, speed is maximized by removing physically impossible discontinuities from model characteristics, carefully controlling coupling between model degrees of freedom, and carefully matching the numerical integration with the equation structure. These considerations have led to a simulation that meets the objectives of accuracy and speed. The aircraft and ship configurations, environmental conditions, and simulation control parameters are specified in a set of input files. The simulation uses this information to describe the physical system. It then generates the time-varying prescribed ship motion and propagates a time-domain solution by numerically integrating the governing equations of motion for the system. An exhaustive set of optional results; includ-

ing aircraft relative angular displacements, securing forces, landing gear reaction forces, suspension forces, tire deflections, induced aerodynamic forces, and animation data; are saved in a selected subset of 18 available output files. Simulation results are post-processed by a suite of utility programs or animated using either two- or three-dimensional animation software tools.

While the forces acting on the aircraft are a function of the aircraft characteristics and the flight deck conditions, the securing forces are largely affected by the securing method. All common aircraft handling systems are included. Model complexity is primarily due to the nonlinearity and range of behaviours associated with the various force-producing elements comprising the model.

DYNAFACE[®] provides the core functionality for aircraft on-deck response simulation. What is required is a good mathematical representation of the skid landing gear.

3. MATHEMATICAL MODELLING

The three main elements required for implementing skid landing gear are the core aircraft dynamics included in DYNAFACE[®], a method for determining suspension deflection resulting from ground loading, and a skid/deck interface model for evaluating ground contact forces. The functional relationship between these models is illustrated in Figure 2. The blocks labelled DYNAFACE and XDOT are the preexisting core functions of the DYNAFACE[®] simulation program. Additional elements PNTGEN, FEMOD, and DCKINT are added to provide skid modelling capability. Block DCKINT is used to evaluate the forces acting at the interface between the skid tubes and the deck. These forces are used to compute the skid landing gear deflections using either a linear stiffness

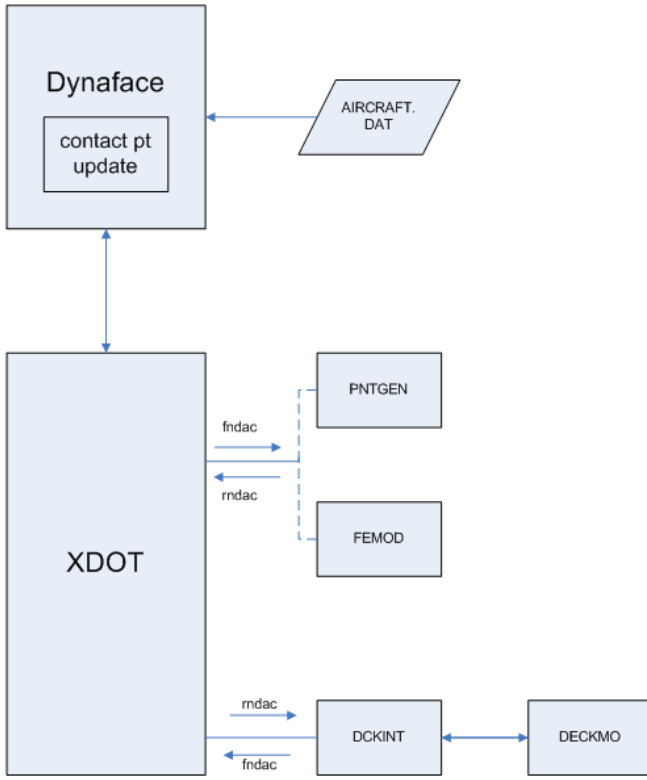


Figure 2. Block diagram of skid modelling approach

modelling approach implemented in PNTGEN or a geometrically nonlinear finite element based approach implemented in FEMOD. Either of these models, whichever is selected, is used subsequently to determine the locations of skid/deck interface nodes which in turn are required for determining the interface forces. Depending upon the resulting magnitudes and directions of these interface forces, the aircraft may remain stationary relative to the ship deck, may slide or yaw on the deck, or may experience relative angular motion resulting in intermittent reduction in vertical contact forces between the skid tubes and deck or in severe cases result in overturning of an unsecured aircraft. All external forces that are modelled within DYNAFACE[®], including rotor inertial and aerodynamic loads as well as applicable securing forces, can be used with the implemented skid landing gear models. Inapplicable securing devices, such as axle spur securing, cannot be used.

3.1. Skid/Deck Interface

The purpose of the skid/deck interface model is to calculate forces applied at nodes used for discretizing the skid tubes along the skid-tube/deck interface. Input to the model con-

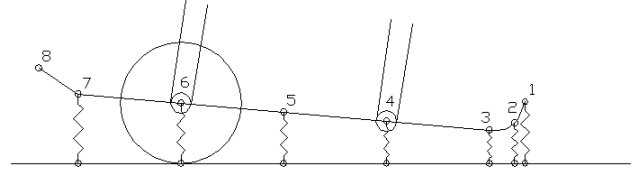


Figure 3. Schematic illustration of skid/deck interface element modelling

sists of nodal position and velocity data and output consists of the three orthogonal force components at each of the nodes. These are expressed in the standard aircraft coordinate frame. Key elements of the model include compression-only springs for determining vertical forces, a friction-slider model for determining the onset of in-plane sliding, distinct stiffness properties at the contact points in the longitudinal and lateral directions, and a viscous damping model representing dissipation at the interface. The input geometric, stiffness, damping, and friction properties are such that ground handling wheels can be accommodated at node locations.

The skid/deck interface model is illustrated in Figure 3. Based on the relative position and velocity between the skid tube nodes and stored deck contact points, the ship frame vertical contact forces are evaluated. The contact force is then used to calculate the maximum frictional force that can be developed between the skid and the deck at the node. The components of the relative displacement and velocity in the plane of the deck are used to determine the corresponding frictional force required to maintain equilibrium and correspondingly no motion of the contact point. In the event that the required force exceeds the allowable friction force, the deck contact point is moved until equilibrium is again satisfied. The forces applied to the nodes are returned to the linear stiffness module or finite element module for subsequent use in determining the suspension deflections.

The relative position vector from each deck contact point to the corresponding node is calculated in global coordinates as

$$\vec{\Delta} = \vec{r}_{deck} - \vec{r}_{node} \quad (1)$$

and similarly the relative velocity vector is calculated as

$$\vec{\dot{\Delta}} = \vec{v}_{deck} - \vec{v}_{node} \quad (2)$$

A vertical force is calculated provided the contact point is in compression, otherwise the vertical force component is set to zero such that

$$F_z = k_z(\Delta_z - \Delta_{z0}) + c_z\dot{\Delta}_z \quad \text{for } \Delta_z - \Delta_{z0} > 0 \quad (3)$$

$$F_z = 0 \quad \text{for } \Delta_z - \Delta_{z0} \leq 0 \quad (4)$$

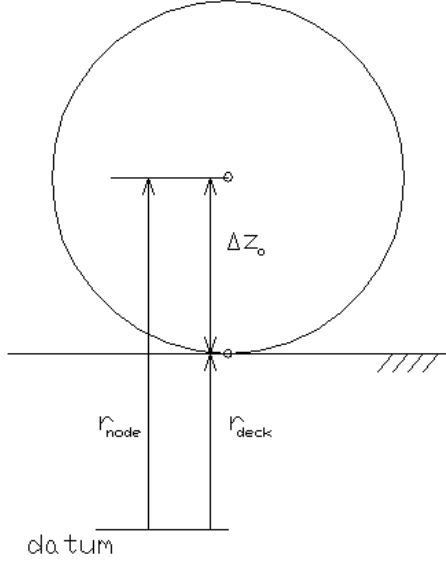


Figure 4. Schematic ground handling wheel geometry

where k_z and c_z are the effective interface contact point linear stiffness and viscous damping coefficients respectively and Δ_{z0} is the undeflected spring length which is used for modelling such devices as ground handling wheels in which case Δ_{z0} is set to the undeflected wheel/tire radius. The geometry associated with ground handling wheels is illustrated in Figure 4.

In the plane of the deck, a frictional slider model is used to track the deck contact point and determine the frictional force components applied to the nodes.

The magnitude of the relative position vector between the projected contact point and the deck contact point in the plane of the deck is determined from

$$\Delta_{act} = \sqrt{\Delta_x^2 + \Delta_y^2} \quad (5)$$

and similarly the relative velocity in the plane of the deck is

$$\dot{\Delta}_{act} = \sqrt{\dot{\Delta}_x^2 + \dot{\Delta}_y^2} \quad (6)$$

The maximum possible friction force is determined from the normal force and the assumed coefficient of friction with the deck as

$$F_{f \max} = \mu F_z \quad (7)$$

The stiffness and viscous damping force components in the plane of the deck are evaluated from the relative displacement from the projected contact point to the actual contact point separately in each component direction. This is necessary to support ground handling wheels by providing different stiffness and damping properties in each direction. The projected contact point is determined by finding the intersection

point between a vertical line in the aircraft frame transformed to the ship frame and the plane of the ship deck. This point will track along the deck in the event that a node lifts away from the deck. However, the projected point will return to the actual contact point prior to contact between the nodal coordinate and the deck. The force that must exist to sustain the relative displacement and velocity is

$$F = k_{act} \Delta_{act} + c_{act} \dot{\Delta}_{act} \quad (8)$$

The actual force cannot exceed the allowable friction force, therefore the force is limited to $F_{f \max}$ such that

$$F_{act} = F_{f \max} \text{ for } F > F_{f \max} \quad (9)$$

The individual force components in the ship coordinate system are determined as

$$\begin{Bmatrix} F_x^{sh} \\ F_y^{sh} \end{Bmatrix} = F_{act} \begin{Bmatrix} \frac{\Delta_x}{\Delta_{act}} \\ \frac{\Delta_y}{\Delta_{act}} \end{Bmatrix} \quad (10)$$

This step effectively allows the deck contact point to slide to the point where the required force does not exceed the in-plane friction limit. The deck contact points, therefore, must be updated to correspond to the allowable contact point locations

$$\begin{Bmatrix} P_x^{sh} \\ P_y^{sh} \end{Bmatrix} = \begin{Bmatrix} P_x^{sh} \\ P_y^{sh} \end{Bmatrix} + \begin{Bmatrix} \frac{\Delta_x}{\Delta_{act}} F_{act} \\ \frac{\Delta_y}{\Delta_{act}} F_{act} \end{Bmatrix} \quad (11)$$

Note that this calculation does not exclusively depend on state variables. The deck contact points must therefore be updated between adaptive time step numerical integration steps. This is represented in Figure 2 by the 'contact pt update' element shown within the DYNAFACE[®] block.

3.2. Linear Structural Stiffness Model

The linear structural stiffness model must accomplish two functions: determine the cross-tube deflections in three dimensions resulting from distributed forces along the skid tubes, and locate each of the skid tube nodes given the calculated cross-tube deflections.

The basic premise of the model is that the linear relationship between the deflections from equilibrium of the ends of each of the cross-tubes and the forces applied at the cross-tube ends is

$$\{F\} = [K] \{\Delta\} \quad (12)$$

or conversely

$$\{\Delta\} = [K]^{-1} \{F\} \quad (13)$$

where

$$\{F\} = \begin{Bmatrix} F_x/2 \\ F_y \\ F_z \end{Bmatrix} \quad (14)$$

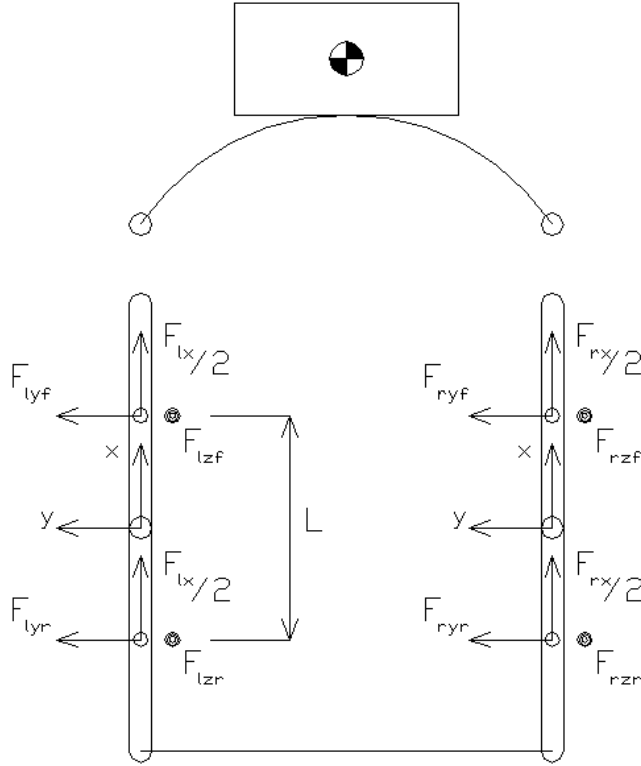


Figure 5. Schematic of skid tube equivalent forces

and

$$\{\Delta\} = \begin{Bmatrix} \Delta_x \\ \Delta_y \\ \Delta_z \end{Bmatrix} \quad (15)$$

Figure 5 illustrates the forces acting at each cross-tube/skid-tube interface. This model, while simple, allows coupling between component directions such that force in one direction can affect deflection in all three component directions.

The force components acting at both cross-tube locations attached to a single skid-tube must be related to the forces acting at each of the skid-tube nodes used to define the skid/deck interface. This is accomplished by performing force balances on each of the skid-tubes and moment balances about the skid-tube vertical and lateral axes passing through the geometrical centre of the tubes. A moment balance about the longitudinal axis of the skid-tube provides no new information; this is why the longitudinal force cannot be discriminated between the front and rear attachment points and is therefore assumed to be shared equally by both cross-tubes. The resulting force and moment balances can be formulated as a system of five linear equations for each of the skid tubes resulting in

$$\begin{bmatrix} 1 & 0 & 0 & 0 & 0 \\ 0 & 1 & 1 & 0 & 0 \\ 0 & 0 & 0 & 1 & 1 \\ 0 & 0 & 0 & a & b \\ 0 & a & b & 0 & 0 \end{bmatrix} \begin{Bmatrix} F_x \\ F_{yf} \\ F_{yr} \\ F_{zf} \\ F_{zr} \end{Bmatrix} = \begin{Bmatrix} -\sum_{i=1}^{N/2} F_{node\ x\ i} \\ -\sum_{i=1}^{N/2} F_{node\ y\ i} \\ -\sum_{i=1}^{N/2} F_{node\ z\ i} \\ -\sum_{i=1}^{N/2} F_{node\ z\ i} \ r_{node\ x\ i} \\ -\sum_{i=1}^{N/2} F_{node\ y\ i} \ r_{node\ x\ i} \end{Bmatrix} \quad (16)$$

where N is the selected total number of skid-tube interface nodes, i refers to individual skid-tube nodes, a is the longitudinal coordinate of the front cross-tube attachment point, and b is the longitudinal coordinate of the rear cross-tube attachment point.

Solving Equation 16 results in all of the force components required to evaluate both of the cross tube deflections on either the left or right sides using Equation 13. This process is repeated for the other skid-tube and associated cross-tubes. It should be noted that the signs of the forces determined from Equation 16 must be reversed prior to their use in Equation 13 based on Newton's third law.

The deflected positions at the ends of each of the cross-tubes, expressed in aircraft-fixed coordinates, can be obtained by adding the cross-tube tip deflections to the undeflected position vectors to the cross-tube ends

$$\vec{r}_i = \vec{r}_{i0} + \begin{Bmatrix} \Delta_x \\ \Delta_y \\ \Delta_z \end{Bmatrix} \quad (17)$$

where i in this case is an index spanning each of the four cross-tubes.

The updated locations of each of the nodes along the skid-tubes can be determined by defining a unit vector pointing from the aft cross-tube/skid attachment point to the forward attachment point for both the left and right skid-tubes

$$\vec{r}_{p\ unit} = \frac{\vec{r}_f - \vec{r}_r}{\|\vec{r}_f - \vec{r}_r\|} \quad (18)$$

The locations of skid tube nodes are specified using a set of coordinate pairs defined as the percentage distance along the skid tubes from the rear attachment point to the front attachment point and an associated elevation for each node above the axis of the skid-tube. The same set of node locations is used for the left and right skid-tubes. The specific coordinate locations can be evaluated by extending the above-defined unit vector from the rear attachment point by the required distance.

This process allows a vector of skid tube node locations $rndac$ expressed in the aircraft coordinate system to be defined for a specific set of skid-tube nodal forces $fndac$.

3.3. Geometrically Nonlinear Structural Stiffness Model

The geometrically nonlinear finite element model provides a comprehensive description of the elastic behaviour of the landing gear structure. In this approach, the landing gear (both cross-tubes and skid-tubes) is discretized and modelled using 2-noded nonlinear beam elements. To account for large deformation and rotation of the landing gear, a geometrically nonlinear stiffness matrix is included in the beam elements based on the Updated Lagrangian framework [7]. The advantage of the geometrically nonlinear finite element model over the linear structural stiffness model is its ability to (i) model different landing gear structure in a unified way, (ii) accurately account for the nonlinear reinforcing or weakening effects resulting from the large deformation and rotations of the landing gear frame, and (iii) calculate the lateral force components in the forward and aft cross-tubes automatically in accordance with their structural stiffness.

The static equilibrium equation of the landing gear in finite element form is

$$\begin{Bmatrix} F_{Cross_tube} \\ F_{Skid_tube} \\ F_{Other} \end{Bmatrix} = \left(\begin{bmatrix} K_{L,CC} & K_{L,CS} & K_{L,CO} \\ K_{L,CS}^T & K_{L,SS} & K_{L,SO} \\ K_{L,CO}^T & K_{L,SO}^T & K_{L,OO} \end{bmatrix} + \begin{bmatrix} K_{NL,CC} & K_{NL,CS} & K_{NL,CO} \\ K_{NL,CS}^T & K_{NL,SS} & K_{NL,SO} \\ K_{NL,CO}^T & K_{NL,SO}^T & K_{NL,OO} \end{bmatrix} \right) \begin{Bmatrix} \Delta_{Cross_tube} \\ \Delta_{Skid_tube} \\ \Delta_{Other} \end{Bmatrix} \quad (19)$$

where subscript ‘Cross.tube’ represents the interface nodes between the aircraft and the landing gear, ‘Skid.tube’ the nodes at the skid/deck interface, and ‘Other’ the other nodes. The linear stiffness $[K_L]$ depends on the geometries, cross-sections, and material properties of the tubes while the nonlinear stiffness $[K_{NL}]$ in general depends on the geometries, initial stresses in the tubes, and deformation of the tubes.

Considering the fact that the external forces acting on nodes other than those on the aircraft/landing gear and skid/deck interfaces are zero, $F_{Other} = 0$, Equation 19 can be simplified using the static condensation procedure [8], such that

$$\begin{aligned} F_{Cross_tube} &= \left[(K_{L,CC} + K_{NL,CC}) - (K_{L,CO} + K_{NL,CO})^T \right. \\ &\quad \left. (K_{L,OO} + K_{NL,OO})^{-1} (K_{L,CO} + K_{NL,CO}) \right] \Delta_{Cross_tube} \\ &\quad + \left[(K_{L,CS} + K_{NL,CS}) - (K_{L,CO} + K_{NL,CO})^T \right. \\ &\quad \left. (K_{L,OO} + K_{NL,OO})^{-1} (K_{L,SO} + K_{NL,SO}) \right] \Delta_{Skid_tube}. \quad (20) \\ F_{Skid_tube} &= \left[(K_{L,SC} + K_{NL,SC}) - (K_{L,SO} + K_{NL,SO})^T \right. \\ &\quad \left. (K_{L,OO} + K_{NL,OO})^{-1} (K_{L,CO} + K_{NL,CO}) \right] \Delta_{Cross_tube} \end{aligned}$$

$$+ \left[(K_{L,SS} + K_{NL,SS}) - (K_{L,SO} + K_{NL,SO})^T \right. \\ \left. (K_{L,OO} + K_{NL,OO})^{-1} (K_{L,SO} + K_{NL,SO}) \right] \Delta_{Skid_tube}. \quad (21)$$

If the interface between the aircraft and landing gear is chosen as the reference, then $\Delta_{Cross_tube} = 0$ and the above equations can be further simplified to

$$F_{Cross_tube} = \left[(K_{L,CS} + K_{NL,CS}) - (K_{L,CO} + K_{NL,CO})^T \right. \\ \left. (K_{L,OO} + K_{NL,OO})^{-1} (K_{L,SO} + K_{NL,SO}) \right] \Delta_{Skid_tube} \quad (22)$$

$$F_{Skid_tube} = \left[(K_{L,SS} + K_{NL,SS}) - (K_{L,SO} + K_{NL,SO})^T \right. \\ \left. (K_{L,OO} + K_{NL,OO})^{-1} (K_{L,SO} + K_{NL,SO}) \right] \Delta_{Skid_tube} \quad (23)$$

Equation 23 is similar to Equation 12 of the linear structural stiffness model except the stiffness is not constant. It determines the relative structural deformation and rotations of the landing gear with respect to the aircraft/landing gear interface. Equation 22, while the first equation determines the forces transmitted to the aircraft through the landing gear. Both equations are nonlinear and the structural stiffness is a function of current stress and deformation of the landing gear.

If the effects of large deformation and rotations of the landing gear are ignored, the above equations are reduced to

$$F_{Cross_tube} = \left[(K_{L,CS}) - (K_{L,CO})^T (K_{L,OO})^{-1} (K_{L,SO}) \right] \Delta_{Skid_tube} \quad (24)$$

$$F_{Skid_tube} = \left[(K_{L,SS}) - (K_{L,SO})^T (K_{L,OO})^{-1} (K_{L,SO}) \right] \Delta_{Skid_tube} \quad (25)$$

where Equation 25 is equivalent to Equation 12 because its stiffness is constant. Thus, it demonstrates that the finite element model can be used to determine the coefficients of the structural stiffness model described in Section 3.2..

3.4. Suspension Damping

Accurate prediction of the aircraft dynamic response requires that skid suspension damping be considered. While the skid-tube/deck interface includes damping, additional damping is required to represent energy dissipation due to suspension deflection or the effect of discrete dampers incorporated in the suspension design. A simple but effective damping model has been implemented to provide damping of the cross-tube deflection. The equivalent forces applied at the skid-tube/cross-tube attachment points are supplemented by damping forces calculated as

$$\{F_d\} = [C] \{\dot{\Delta}\} \quad (26)$$

where $[C]$ is defined using the first term of the Caughey series resulting in the relationship

$$[C] = a_0 [K] \quad (27)$$

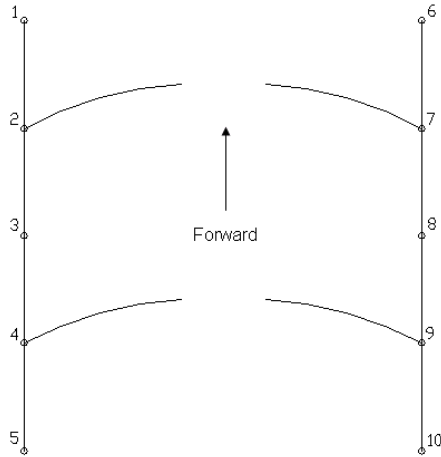


Figure 6. Node layout for linear model example

where $[K]$ is the effective cross-tube 3×3 stiffness matrix. These matrices are directly input for the linear stiffness model for each cross tube. For the purpose of stiffness calculation using the finite element model, no such matrices are directly input; rather, the global stiffness matrix is assembled internally. However, for the purpose of the damping calculation, separate representative damping matrices are input through the deck interface portion of the finite element input file.

3.5. Implementation and Verification

The mathematical model, in the form described, was implemented, verified, and interfaced to the DYNFACE[®] simulation program. Once integrated, the model was verified prior to its application. Numerous cases have been simulated to investigate the performance of the skid landing gear models and the associated skid/deck interface model. This section presents two sets of sample results: a simulated drop test and a test of the onset of sliding.

The drop test was simulated by allowing the aircraft body to have six degree-of-freedom motion when released from rest after being raised approximately 0.3 feet from its static equilibrium position and orientation on the deck. The node locations used with the linear model employed in this case are shown in Figure 6. This preliminary run used a value of $a_0 = 0.02$. The results for heave and pitch motion are shown in Figure 7. As can be seen, the system quickly returns to equilibrium after a short period of heavily-damped oscillation.

A different set of drop test conditions was used to demonstrate how the damping coefficient affects the rate of energy dissipation and the shape of the resulting transient. Drop test results for three different values of a_0 are shown in Figure 8.

The next test again used the linear stiffness model and an

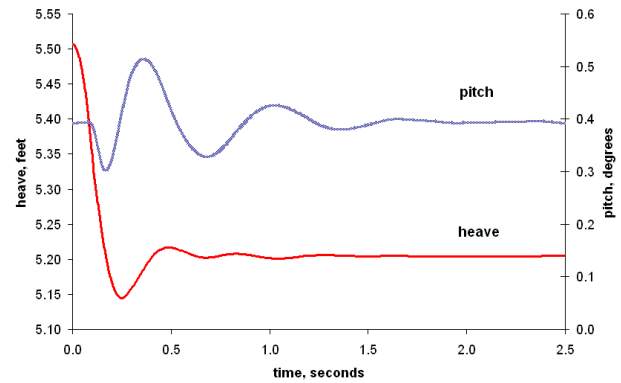


Figure 7. Linear model drop test results

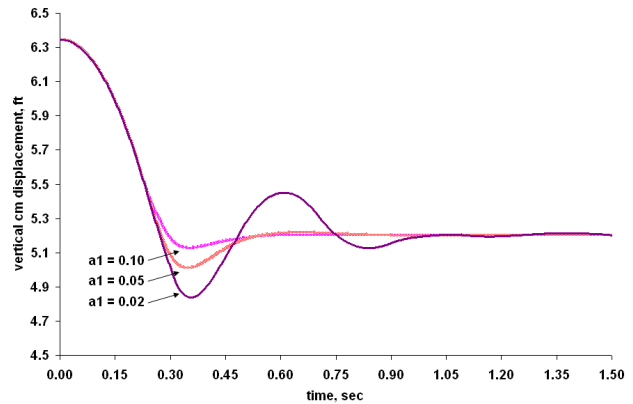


Figure 8. Effect of stiffness proportional damping coefficient a_0

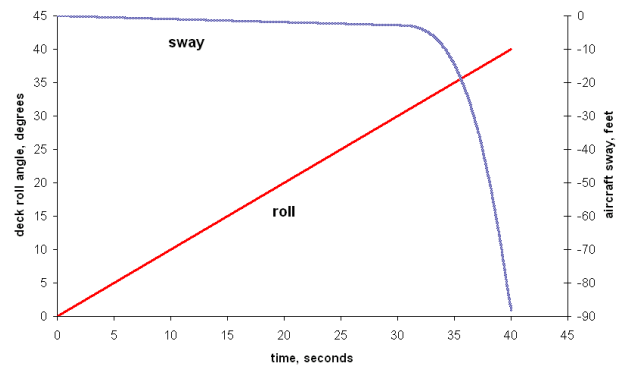


Figure 9. Prediction of the onset of aircraft sliding with linearly increasing deck roll angle

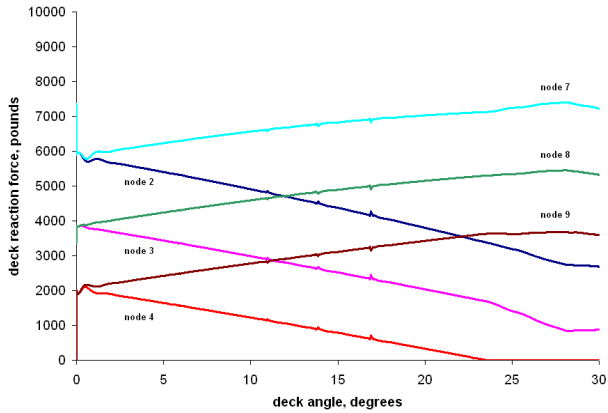


Figure 10. Variation of skid/deck interface reaction forces with linearly increasing deck roll angle

unsecured aircraft. The deck motion was prescribed to increase linearly in roll at a rate of 1 degree per second. Figures 9 and 10 show the results for aircraft centre of mass lateral position and skid-tube/deck node interface forces respectively. The displacement plot shows that sliding initiates close to a deck angle of 31 degrees as it should for a deck coefficient of friction of 0.6 that was used in the simulation. The force results showed that the front and back nodes on each skid that were elevated from the deck due to skid-tube upward curvature at the ends did not develop vertical force in the simulation. The three middle nodes on each skid have greater values toward the front of the aircraft due to the forward location of the aircraft centre of mass. As the deck angle increases, the vertical reaction forces on the lower side (right/starboard) increase and conversely for the upper side. This is what is expected as the up-slope skid unloads as the line passing through the aircraft weight vector intersects the deck increasingly close to the right skid as the deck roll angle increases.

These results, combined with others not presented, confirm the correction functioning of the linear suspension stiffness and damping model as well as the skid/deck interface model.

4. SAMPLE APPLICATION

This section presents a simulation of a typical skid-equipped aircraft using the linear modelling approach presented in this paper.

4.1. Aircraft Response Analysis

DYNAFACE[®] was developed as a versatile analysis tool capable of performing various types of analyses including model development, on-deck performance analysis, fatigue analysis, clearance analysis, and parameter optimization. Unlike naval aircraft with traditional tricycle type landing gear,

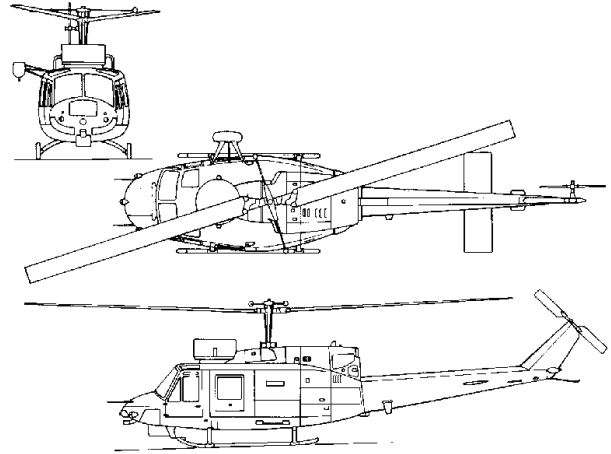


Figure 11. Front, top, and side views of an AB-212 helicopter [9]

skid type aircraft require extra precautions when operating on the flight deck of a moving naval platform. It is with this added need for caution that the modelling of skid aircraft in computer simulations becomes important. This section describes a simple on-deck aircraft response analysis of a shipborne skid type aircraft, represented by an AB-212, operating from a typical frigate. The plan view of a typical AB-212 helicopter is shown in Figure 11.

4.2. Simulation Methodology

The specific character and magnitude of skid reaction forces and deflections vary considerably and are dependent upon aircraft configuration, ship operating conditions, and environmental conditions. Aircraft configuration includes parameters such as aircraft mass properties (maximum take-off, minimum landing), centre of mass location (forward-most, aft-most), rotor status (stopped or turning), kinematic properties of skids and cross tubes (stiffness and damping), aircraft alignment with respect to the ship's centreline, and aircraft location on the ship (flight deck or hangar). Ship operating conditions include heading and speed relative to the principle wave direction. Environmental conditions include sea state (SS), wind speed, wind direction, and geographic location. Also, the type of aircraft-embarked operation can vary; possibilities include: touchdown, free-deck analysis, on-deck securing, aligning for hot refuelling and rearmament, straightening, traversing, and stowage in the hangar. In a detailed simulation study, an aircraft may operate in conditions characterized by all combinations of these parameters. However, for the purpose of this paper two cases will be presented.

Table 1. Simulation conditions used

Parameter	Value
Aircraft weight	10600 lbf
Rotor status	Turning
Aircraft alignment	centred
Skid type	Aluminium, circular cross-section
Ship speed	5 knots
Ship headings	60 degrees
Significant Wave Height (SWH)	1.25 m (SS 3), 4 m (SS 5)
Wave modal period	9.0 sec for SWH of 1.25 m 10.9 sec for SWH of 4 m
Wind speed	Sea State 3 = 20 knots, Sea State 5 = 35 knots
Wind direction	Port beam

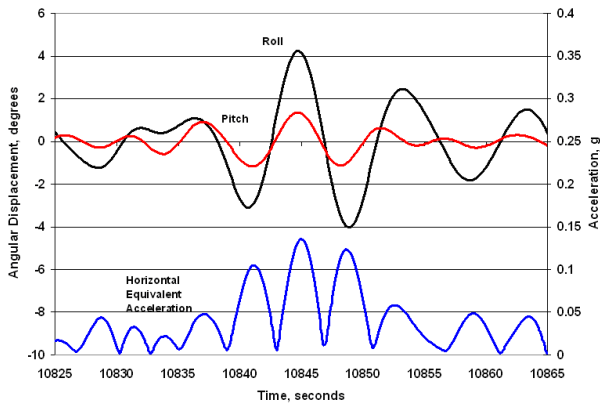


Figure 12. 40-second ship motion time history corresponding to sea state 3

4.3. Simulation Conditions

Table 1 summarizes the simulation cases considered. For each of the two simulation cases, the ship motion corresponds to the occurrence of the peak in-plane (horizontal) flight deck equivalent acceleration. For the purpose of this demonstration, ship motion was generated using established linear strip theory for a 4700 tonne frigate. Alternatively, DYNAFACE[®] could use actual recorded ship motion as input.

4.4. Simulation Results

Time histories of the forces and relative displacements that result at the dynamic interface between the skid type aircraft and the typical frigate considered were predicted using DYNAFACE[®]. Figures 12 and 13 show 40-second periods of ship motion corresponding to the 4700 tonne frigate at a

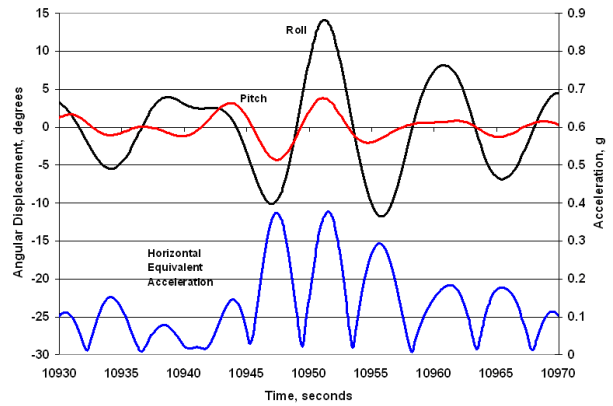


Figure 13. 40-second ship motion time history corresponding to sea state 5

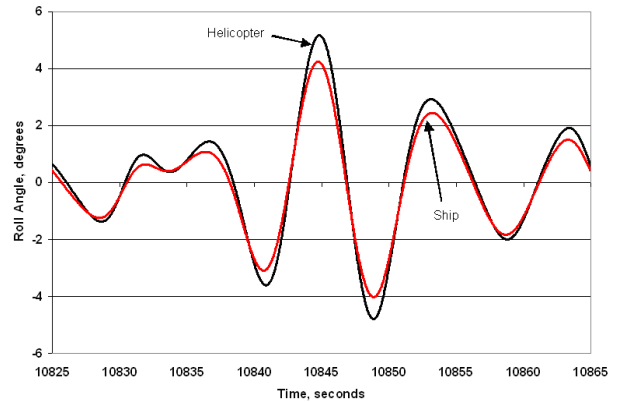


Figure 14. Aircraft and ship roll angles in sea state 3

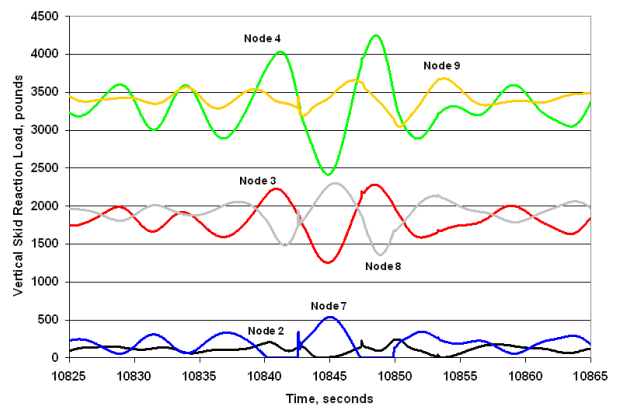


Figure 15. Vertical skid reaction forces in sea state 3

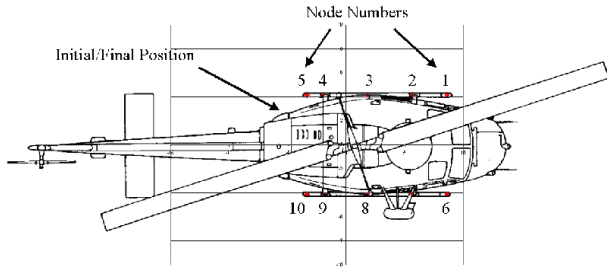


Figure 16. Skid in-plane displacements in sea state 3

speed of 5 knots and a heading of 60 degrees in sea state 3 and sea state 5 respectively corresponding to littoral waters of the North Atlantic Ocean. The aircraft is located at the centre of the designated landing area for which the aircraft response analyses were performed.

The ship motion combined with the aircraft configuration summarized in Table 1 produced time histories of skid reaction forces and aircraft displacements during a typical embarked operation corresponding to an unsecured aircraft otherwise known as free-deck operations. Figures 14 through 16 show the ship and aircraft roll angles, skid vertical reaction forces, and aircraft linear displacements respectively for the sea state 3 case. As can be seen, the predicted aircraft response in roll follows the ship roll response. The relative angle that exists is expected and is primarily due to the kinematic characteristics of the cross-tube suspension. The small peak relative roll magnitude of less than 1 degree is also expected. From experience, tricycle type landing gear suspension systems are less stiff than the skid cross tubes allowing for larger suspension travel and therefore larger relative angles. Analysis of the vertical reaction load plot (Figure 15) shows the force characteristics agree with the ship motion in that the up-slope skid becomes lightly loaded when the ship is rolled to starboard and vice versa. Refer to the node numbering convention in Figure 6. Note that nodes 1, 5, 6, and 10 do not experience any loads as the skids have an upward curvature at their ends (refer to Figure 11) and the ship motion is insufficient to cause the aircraft to have these nodes contact the deck. The higher loading on nodes 4 and 9 are expected as the longitudinal centre of mass location is in the vicinity of the rear cross tubes. Due to the relatively benign ship motion no change in aircraft displacement was observed as shown in Figure 16.

Figures 17 through 19 show the ship and aircraft roll angles, skid vertical reaction forces, and aircraft linear displacements respectively for the sea state 5 case. As with the sea state 3 example, the predicted aircraft response, in roll, follows the ship roll response. The peak relative roll is slightly larger (less than 3 degrees) as compared to the sea state 3 example due to the higher ship motion amplitude. Analysis

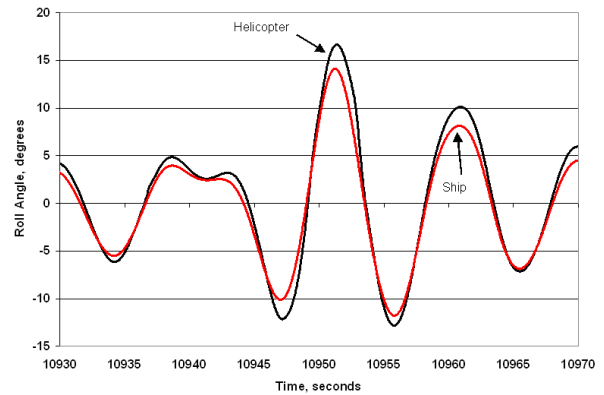


Figure 17. Aircraft and ship roll angles in sea state 5

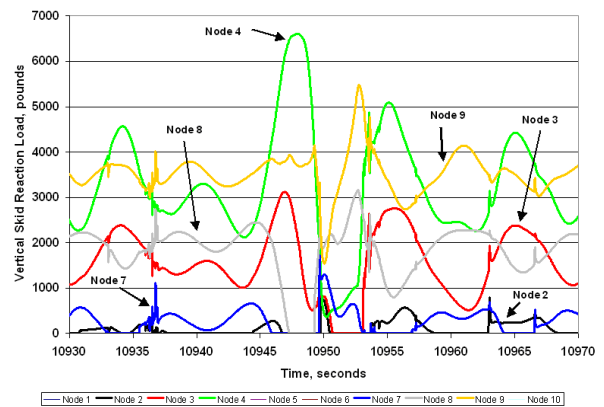


Figure 18. Vertical skid reaction forces in sea state 5

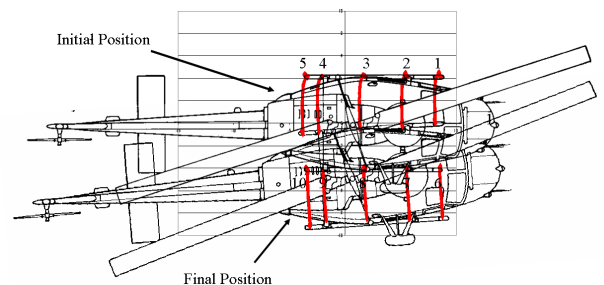


Figure 19. Skid in-plane displacements in sea state 5

of the vertical reaction load plot (Figure 18) shows the force characteristics agree with the ship motion in that the up-slope skid becomes lightly loaded when the ship is rolled to starboard and vice versa. Again, nodes 1, 5, 6, and 10 do not experience any loads due to the upward curvature of the skid ends and the ship motion is insufficient to cause the aircraft to have these nodes contact the deck. With the increase in ship motion severity, instances of the skids coming off the deck become apparent. As a result, translation displacements of the aircraft can be expected as can be seen in Figure 19 where during the 40-second simulation run, the aircraft has laterally translated across the flight deck approximately 4 feet and yawed approximately 4 degrees. The results of this support the requirements for an aircraft securing system where otherwise restricting aircraft operations is not desirable.

5. CONCLUSION

This paper presented the extension of the DYNAFACE[®] dynamic interface analysis software tool to include the modelling of skid landing gear. Verification results as well as experience with analysis of representative skid-equipped aircraft confirm the utility of the model. This allows DYNAFACE[®] to be applied to a new class of problem and to further contribute to improving the safety of shipboard aircraft operation.

REFERENCES

- [1] R. G. Langlois, M. LaRosa, and A. R. Tadros. Development, Validation, and Application of the Dynaface Helicopter/Ship Dynamic Interface Simulation Software Package. In *SCSC 2003 Summer Computer Simulation Conference*, Montreal, QC Canada, July 2003. The Society for Modeling and Simulation International.
- [2] R. G. Langlois and A. R. Tadros. *User's Manual for the Aircraft/Ship Dynamic Interface Simulation Dynaface Release 5.0*. Indal Technologies Inc., Mississauga, Ontario, Canada, January 1998. ITI Report No. 99/419.
- [3] I. Sharf and L. Monterrubio. Influence of landing gear design on helicopter ground resonance. In *Proceeding of the AIAA Modeling and Simulation Technologies Conference and Exhibit*, Portland, Oregon, USA, August 1999.
- [4] B. E. Stephens and W. L. Evans, Application of Skid Landing Gear Dynamic Drop Analysis. In *Proceedings of the American Helicopter Society 55th Annual Forum*, Montreal, Quebec, Canada, May 1999.
- [5] C.-H. Tho, C. E. Sparks, A. K. Sareen, M. R. Smith, and C. Johnson, Efficient Helicopter Skid Landing Gear Dynamic Drop Simulation Using LS-DYNA. In *Proceedings of the American Helicopter Society 59th Annual Forum*, Phoenix, Arizona, May 2003.
- [6] MD Helicopters Inc. Rotorcraft maintenance manual: Landing gear assembly description and operation. Technical Report CSP-900RMM-2,32-00-00, MD Helicopters, Inc., Mesa, Arizona, 2003.
- [7] Z. H. Zhu and S. A. Meguid. Elastodynamic analysis of low tension cables using a new curved beam element. *International Journal of Solids and Structures*, 43:1492–1504, 2006.
- [8] K. J. Bathe. *Finite Element Procedures*. Prentice Hall Inc., 1996.
- [9] The-Blueprints.com. Agusta Bell AB-212 ASW. Online-<http://www.the-blueprints.com/index.php?blueprints/modernplanes/heli-a-b/1729/view/>; Accessed November 13, 2007.

Info

curtisswrightds.com

Email

ds@curtisswright.com